The Mechanics of a Cantilever Beam with an Embedded Horizontal Crack Subjected to an End Transverse Force, Part A: Modelling

Panos G. Charalambides, Xiaomin Fang

The Mechanics of a Cantilever Beam with an Embedded Horizontal Crack Subjected to an End Transverse Force, Part A: Modelling[a]

Panos G. Charalambides[1b] and Xiaomin Fang[1]

1 – Department of Mechanical Engineering, The University of Maryland, Baltimore County,1000 Hilltop Circle, Baltimore, MD 21250, USA

DOI **10.13140/RG.2.1.3874.4560**

Keywords: Cantilever, beam, model, embedded, horizontal, crack, mechanics, modelling.

ABSTRACT. This study addresses the mechanics of a cracked cantilever beam subjected to a transverse force applied at it's free end. In this Part A of a two Part series of papers, emphasis is placed on the development of a four-beam model for a beam with a fully embedded horizontal sharp crack. The beam aspect ratio, crack length and crack centre location appear as general model parameters. Rotary springs are introduced at the crack tip cross sections as needed to account for the changes in the structural compliance due to the presence of the sharp crack and augmented load transfer through the near-tip transition regions.

Guided by recent finite element findings reported elsewhere, the four-beam model is advanced by recognizing two key observations, *(a) the free surface and neutral axis curvatures of the cracked beam at the crack center location match the curvature of a healthy beam (an identical beam without a crack under the same loading conditions), (b) the neutral axis rotations (slope) of the cracked beam in the region between the applied load and the nearest crack tip matches the corresponding slope of the healthy beam.* The above observations led to the development of close form solutions for the resultant forces (axial and shear) and moment acting in the beams above and below the crack. Axial force and bending moment predictions are found to be in excellent agreement with 2D finite element results for all normalized crack depths considered. Shear force estimates dominating the beams above and below the crack as well as transition region length estimates are also obtained. The model developed in this study is then used along with 2D finite elements in conducting parametric studies aimed at both validating the model and establishing the mechanics of the cracked system under consideration. The latter studies are reported in the companion paper Part B-Results and Discussion.

Introduction. Over the last two decades, the frequency response [1-5] of a component or a structure has been used to assess "structural health" as one of several methods used in damage detection [6-13] and structural health monitoring. In most of such studies, the effects of damage on the structural frequency response has been explored using a cantilever beam geometry. With the above in mind, diffused damage detection studies have been developed [7-13] using optimization algorithms that minimize an "error estimate". Typically, the employed "error estimates" are calculated by comparing the experimentally measured frequencies of the structure [8] to the respective frequencies predicted by a physics based model that solves a problem of the same structural geometry but with reduced localized properties at a prescribed location [9]. Often, the optimization algorithms identify the model structure that best matches the experimental results, thus identifying the likely location and degree of structural damage manifested through the EI, structural stiffness reduction. For example, Xu *et al*. [8] developed a damage detection algorithm that monitors the changes in the first 10 transverse frequencies of a vibrating beam as a means of detecting the location and degree of damage along the axis of the beam as measured through a reduced localized structural stiffness. The promising outcomes of their initial studies have been validated through model experiments and have sparked

[a] This research was partially supported through a University of Maryland, Baltimore County DRIF award and Graduate Assistantship in the Department of Mechanical Engineering.
[b] Professor Charalambides would like to acknowledge many useful discussions with Mechanical Engineering Professor Weidong Zhu and Professor Emeritus Christian von Kerczek.

new interest in expanding the studies to include detection of diffused damage in more complicated structures such a frames and bolted joints [11-15].

While the above efforts address damage assumed to be diffused over a prescribed region, in recent years a few studies have attempted to address the effects of sharp cracks on the modal response of a structure [16-27], a few of which employ basic fracture mechanics concepts [22-27]. Such studies require prior knowledge of the fracture mechanics stress fields and related stress intensity factors. The near-tip fracture quantities are thought to be required in assessing the energy changes due to the introduction of a crack and the related changes in the structural compliance or associated stiffness changes induced by the presence of a sharp crack. As a result, fracture mechanics based studies have been limited to systems with edge cracks for which the stress intensity factors [28-32] dominating the crack tip region is known. Furthermore, most such studies also assume the presence of a mode I "breathing" crack thus preserving the linearity of the system that would otherwise be violated due to non-linear crack surface contact effects. More recently, Jing *et al.* [27] employed a variation of the model presented in this work in obtaining the natural frequencies of a cantilever beam containing a horizontal crack capable of relative crack surface sliding but not opening.

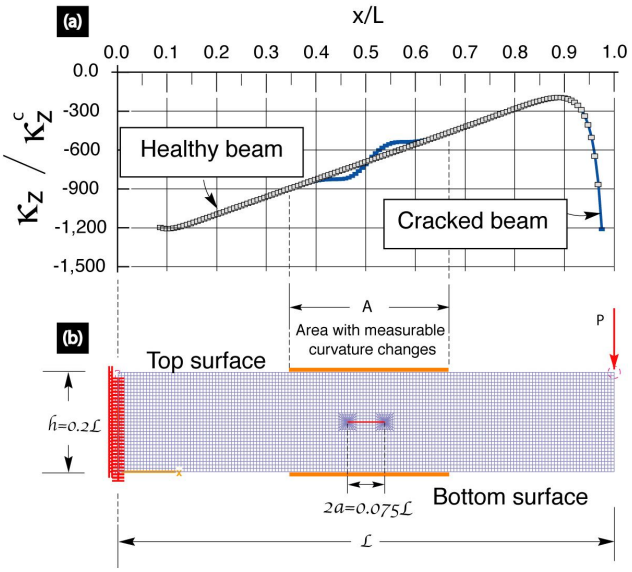

Fig. 1. Normalized top surface beam curvatures for a healthy and cracked beams generated using 2D finite elements.

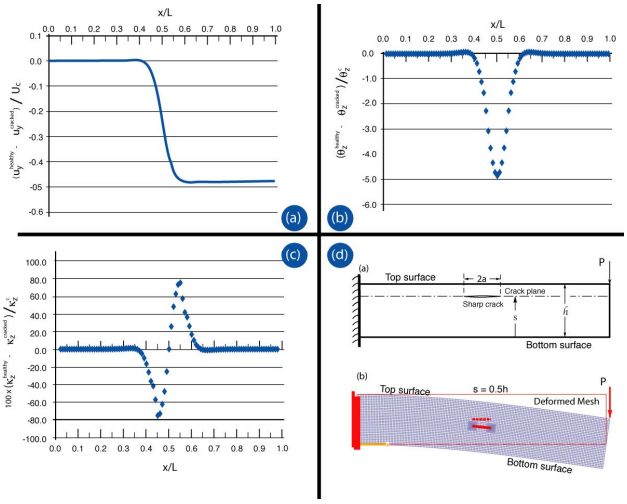

Fig. 2. Normalized (a) deflections, (b) slope and (c) curvature differences between a cracked and a "healthy" beam subjected to an end loading P.

Recently, Two-Dimensional (2D) Finite Element (FE) studies [33-35] on the cantilever specimen shown in Figs. 1-4, suggest that predominately mode II conditions dominate both crack tip regions for a fully embedded horizontal sharp crack subjected to the loading conditions shown in Fig. 1b. As such, and under ideally flat crack surface condition, surface contact should minimally affect the overall load transfer and deformation mechanics of the specimen shown in Fig. 3. Furthermore, finite element findings reported in [33, 34] (see Figs. 1-3) led to the following two key observations; *(a) the free surface and neutral axis curvatures of the cracked beam at the crack center location match the curvature of a healthy beam, i.e., an identical beam without a crack under an end force condition, and (b) the neutral axis rotations (slope) of the cracked beam in the region between the applied load and the nearest crack tip matches the corresponding slope of the healthy beam.*

Guided by the above finite element findings, in this study a four-beam model [33] is developed in an effort to establish simple but effective physics based models capable of predicting the load transfer and deformation mechanics as well as the near tip fracture conditions, the frequency and modal

response of structures with fully embedded cracks of the type shown in Fig. 4. The development of the four-beam model shall be presented next.

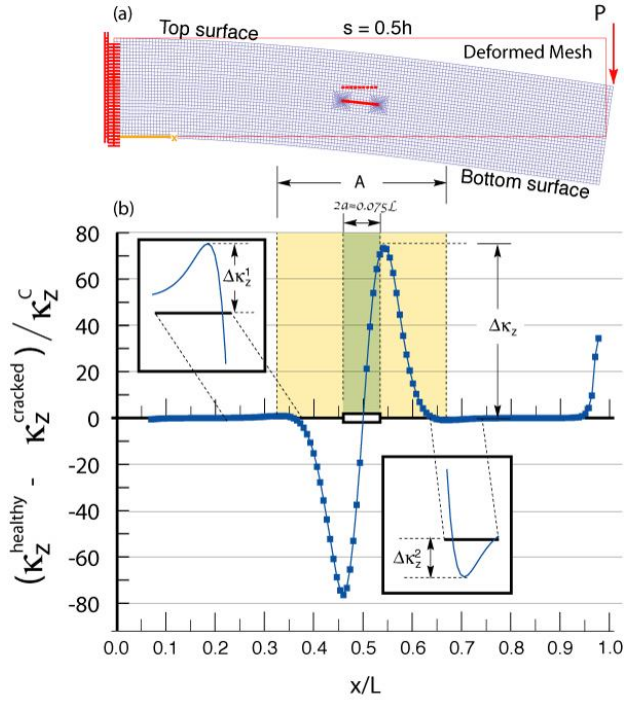

Fig. 3. Normalized curvature differences between a cracked and a healthy beam extracted for the top beam surface using 2D finite element models. In this simulation for the cracked beam, a horizontal sharp crack of normalized length $2a = 0.15L$ was placed at the center of the beam as shown in (a) above. The beam aspect ratio used was $h/L = 0.2$. The results support the existence of transition regions of equal length at the left and right crack tips.

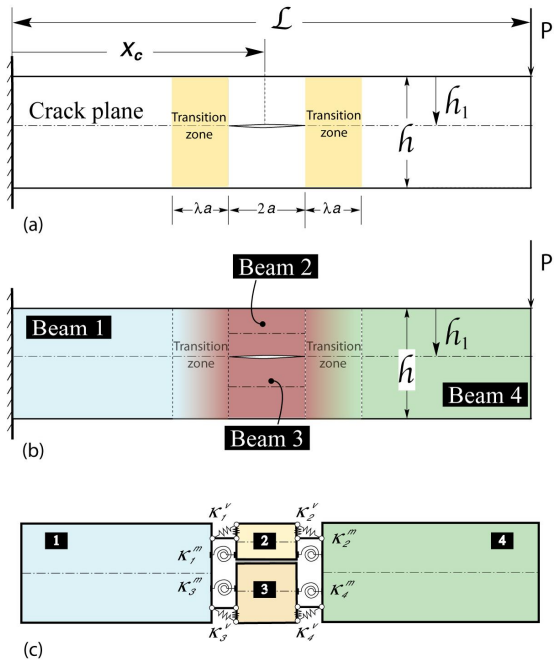

Fig. 4. Schematics highlighting the four beam model development. Rotary springs are introduced at the interfaces between beams 1 and 2, 2 and 4, 1 and 3, and 3 and 4. (a) A schematic showing the geometry and boundary conditions applied on the cracked beam. (b) The identification of the four beams. (c) The four beams connected through rotary springs at their interfaces.

Development of the four-beam model. The results presented in Figs. 1-3 were obtained as part of a broad finite element study aimed at establishing the deformation and fracture mechanics of a cantilever beam containing a fully embedded sharp crack positioned at any admissible location and orientation within the beam domain. The results of those studies are reported in greater detail elsewhere [33]. In Fig. 1, the curves shown represent the curvatures of a healthy and a cracked beam extracted from respective finite element models at the top beam surfaces. As indicated in Fig. 1, the results correspond to a beam of aspect ratio $L/h = 5$, with the cracked beam containing a horizontal through thickness sharp crack of length $l = 0.075L$ located at the center of the beam at $x_C = 0.5L$. The curvature results for the healthy beam i.e., a beam without a crack but otherwise geometrically identical to the one with the crack, are represented by the rectangular open symbols. As expected, away from the ends, the healthy beam curvatures form a linear profile with position x consistent with the bending theory prediction of $d^2y/dx^2 = M(x)/EI$, where $y(x)$ represents the deflection of the beam neutral axis, $M(x)$ is the bending moment at location x, E is the elastic modulus and I is the second moment of inertia with respect to the bending axis. On the other hand, the top surface curvatures predicted for the cracked beam are shown using the solid blue symbols. As shown in Fig.

1, the curvature results for the cracked beam deviate from those of the healthy beam only in the crack region exhibiting a sinusoidal-like profile over a distance A that appears to be approximately two to three times the crack length size. Most importantly for this study, one observes that the curvature of the cracked beam intersects the healthy beam curvature profile at the center of the crack consistent with Figs. 1-3. This observation has been validated through broad parametric studies reported in [33]. In fact, the observation has been found to hold true for curvature estimates for the top and bottom beam surfaces as well as for the mid-planes above and below the crack in the crack region. Informed by the above observations, the following hypothesis used in constructing the proposed four-beam model is put forward.

Proposed deformation hypothesis. *For any cantilever beam system containing a horizontal sharp crack and subjected to an end transverse loading, the curvatures of the mid-planes above and below the crack match the curvature of the healthy beam at the crack center location.*

Guided by the above observation, let's consider the cracked cantilever beam shown in Fig. 4a. The beam has a length L, height h while containing a horizontal sharp crack of length $l = 2a$ located at position x_C from the fixed end at depth h_1 from the top surface. In this study, the above domain is divided into four sub-domains, each forming a beam as shown in Fig. 4b labeled Beam-1, Beam-2, Beam-3 and Beam-4. As will be discussed later on in this work and as suggested by finite element studies reported in [33] and in Figs 1-3, a transition region exists between Beam-1 and Beams 2 and 3 at the left crack tip and the same Beams 2 and 3 and Beam-4 at the right crack tip. While the effects of the transition regions will be incorporated into the four-beam model, at present we shall focus on the mechanics of Beams 2 and 3 since their response appears to be directly linked to the deformation hypothesis stated above. More specifically, let's consider the beam free body diagrams shown in Fig. 5.

As shown, at the crack center cross sections, Beam-2, i.e., the beam above the crack plane, is subjected to an axial force resultant N_t, shear force resultant V_t and bending moment resultant M_t. Similarly, Beam-3 also referred to in this study as the bottom beam denoted by a subscript b, is subjected to force and moment resultants N_b, V_b and M_b respectively. Meanwhile, Section/Interface 1, which is the left end of the top beam, is subjected to the force and moment resultants N_1, V_1 and M_1 whereas the right end of the same beam is subjected to N_2, V_2 and M_2 at Interface 2. Similarly, the bottom beam or Beam-3 is subjected to end forces and moments N_3, V_3 and M_3 at Section/Interface 3 and N_4, V_4 and M_4 at Section 4 as shown in Fig. 5c.

Based on the proposed deformation hypothesis, the curvature of Beams 2 and 3 at the center of the crack should be equal to the curvature of the healthy beam, i.e.,

$$\frac{d^2 y_2}{dx^2} = \frac{d^2 y_3}{dx^2} = \frac{d^2 y}{dx^2} \text{ at } x = x_c \tag{1}$$

where $y_2(x)$ – is the mid-plane deflection of Beam 2;

$y_3(x)$ – is the mid-plane deflection of Beam 3;

$y(x)$ – is the mid-plane deflection of the healthy beam.

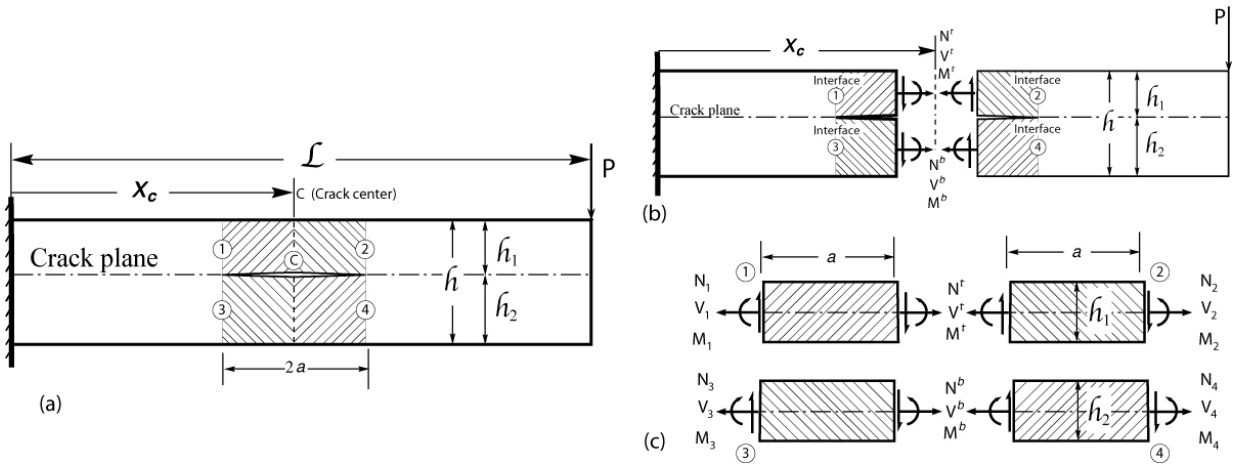

Fig. 5. Schematics used in the development of the analytical model capturing the mechanics of the beams above and below the crack, i.e., Beams 2 and 3 shown in Fig. 4. (a) The cracked beam with Beams 2 and 3 highlighted along with Interfaces 1-4. (b) A section through the center of the crack exposing the force and moment resultants acting in the "top" and "bottom" beams. (c) Free body diagrams of the left and right half of the "top" and "bottom" beams, exposing the resultants acting at their corresponding Interfaces 1-4.

Consistent with beam theory [36-37], it can be shown that the above differential equations can be expressed in terms of the bending moments acting in each beam at the cross section of interest and the bending stiffness *El* for each beam, i.e.,

$$\frac{M_t}{El_t} = \frac{M_b}{El_b} = \frac{M_c}{El} \tag{2}$$

where the subscripts *t* and *b* denote quantities for the top (Beam 2) and bottom (Beam 3) beams respectively.

The above simple equations for the moment resultants at the center of the crack are general, in that, they yield the moment resultants in the top and bottom beams at the center of the crack as a function of the bending moment experienced by the healthy beam at the same location, i.e.,

$$M_t = \frac{l_t}{l} M_c \text{ and } M_b = \frac{l_b}{l} M_c \tag{3}$$

where for a downward load *P* the bending moment at the crack center location in the healthy beam is $M_c = -P(L-x)$. With the bending moments acting in the top and bottom beams know, an expression for the axial forces N_t and N_b is then obtained through a global moment equilibrium enforced over the right half of the beam (see Fig. 5b), such that,

$$\Sigma M_c = 0 \text{ yields } N_t \frac{h_1}{2} - N_b \frac{h_2}{2} - M_t - M_b + M_c = 0 \tag{4}$$

Force equilibrium in the *x* direction for either half of the beam shown in Fig. 5b results in the obvious outcome that the axial force in the bottom beam should be equal and opposite to its counterpart acting

in the top beam, i.e., $N_b = -N_t$. The latter finding along with Eqns (3) and (4) yield a general expression for the axial forces N_t and N_b as follows,

$$N_b = -N_t = \frac{2M_C}{h}\{1 - \frac{I_t+I_b}{I}\} \tag{5}$$

where I, I_t and I_b are the second moments of inertia with respect to the bending axis of the healthy beam, top beam or Beam-2 and bottom beam or Beam-3 respectively;

h – is the beam height

M_c – as before is the bending moment acting at the crack center location in the healthy beam.

Further enforcing force equilibrium in the y direction for either half of the beam shown in Fig. 5 yields,

$$V_t + V_b = P \tag{6}$$

Now, by enforcing force and moment equilibrium within the top and bottom beams shown in Figs. 5c and 6a, one can easily establish the following relations between the cross sectional resultants acting at the beam interfaces 1, 2, 3 and 4 shown in Fig. 5c,

$$\begin{array}{llll} N_1 = N_t & N_2 = N_t & N_3 = N_b & N_4 = N_b \\ V_1 = V_t & V_2 = V_t & V_3 = V_b & V_4 = V_b \\ M_1 = M_t - V_t a & M_2 = M_t + V_t a & M_3 = M_b - V_b a & M_4 = M_b + V_b a \end{array} \tag{7}$$

The above analysis suggests that in the presence of a horizontal crack, load transfer across the cracked cross section is enabled by the development of a force couple subjecting the beams above and below the crack into compression and tension respectively for an upwardly applied load P. Meanwhile, the same beams experience a linearly varying bending moment between Interfaces 1 and 2 for the upper beam and 3 and 4 for the lower beam. In the same interval, and over the length of each beam which is equal to the length of the horizontal crack, both the axial and shear resultant forces $N(x)$ and $V(x)$ remain constant and equal to the values attained at the crack center cross sections. Thus far, the shear force resultants V_t and V_b dominating the top and bottom beams are the only remaining unknowns in determining the load transfer mechanics across the beam crack region. These quantities are established below along with other problem variables using beam compatibility conditions.

Beam compatibility conditions. Compatibility conditions are required in enforcing displacement and cross sectional rotation conditions at the interfaces between two beams. It is common to cast a beam problem using the second order differential equation of the elastic curve of the beam along with deflection and beam slope boundary and matching conditions. In this study, for simplicity purposes we shall employ the method of linear superposition in addressing the deformation mechanics of the four-beam model presented in Fig. 4. More specifically, in this formulation each beam will be treated as a Timoshenko beam thus accounting in the general formulation for shear effects. The deformation of each beam (deflections, cross sectional rotations and slope of neutral axis, will be accounted for by superimposing the local deformations of a cantilever beam subjected to end transverse force V and moment M shown in Fig. 6b, to the deformations caused by the deflection and rotation of the "fixed" attached to its adjacent deforming beam. In doing so, the deflection δ, cross section rotation

φ and slope of the neutral axis ϑ at the free end of a typical Timoshenko beam shown in Fig. 6b will be used. For a beam of constant cross section, homogeneous material properties and the loading shown in Fig. 6b, the above quantities are given by [37],

$$\delta = -\frac{VL^3}{3EI} - \frac{VL}{kAG} + \frac{ML^2}{2EI}, \text{ – Deflection at Free End}$$
$$\varphi = \frac{VL^2}{2EI} + \frac{ML}{EI}, \text{ – Rotation of Cross Section at Free End} \quad (8)$$
$$\vartheta = -\frac{VL^3}{2EI} + \frac{ML}{EI} - \frac{V}{kAG} \text{ – Beam Slope at Free End}$$

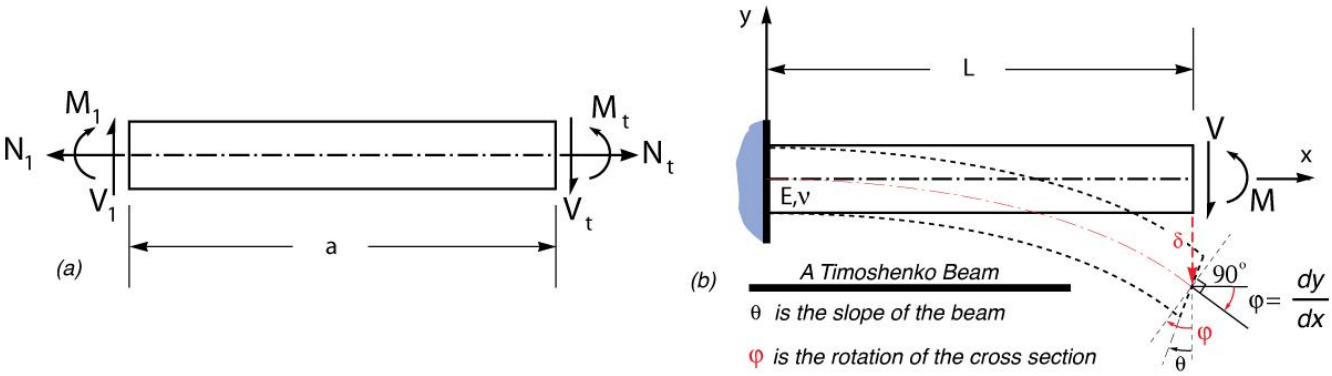

Fig. 6. (a) A free body diagram of the left half of the "top" beam or Beam-2 showing the force and moment resultants acting at interface 1 and mid-section at the crack center. The above schematic along with similar schematics shown in Fig. 5 were used in obtaining the equilibrium equation (7). (b) A Timoshenko cantilever beam subjected to end transverse force V and moment M loading. The deformed configuration is drawn to distinguish between the beam slope ϑ at the free end and the rotation of the cross section denoted by φ used in the compatibility equations.

Where the Timoshenko constant κ [38] appears to influence the deflection δ and slope ϑ, but not the rotation of the cross section measured by φ. For clarity purposes, it may be important to note that in a Euler-Bernoulli [39] beam, the deformed cross section remains perpendicular to the neutral axis and thus its rotation is equal to the slope of the beam. However, due to shear effects, in a Timoshenko beam the normal to the deformed cross section may not align with the deformed neutral axis and thus φ may not be equal to ϑ as suggested by Eqn. (8) above and shown schematically in Fig. 6b. With the above in mind, the compatibility at beam interfaces put forward below will be enforced on the cross sectional normal φ and not on the beam slope ϑ which may exhibit discontinuities at beam interfaces due to shear effects.

Introduction of "Transition Regions". Supported by 2D finite element studies [33], a key contribution of this study is the hypothesis that load transfer through Interfaces 1 through 4 shown in Fig. 5b, takes place in a more convoluted manner within relatively confined transition regions at each of the four-beam interfaces as shown schematically in Figs. 4, 7 and 8. In fact, as will be discussed in this section, the load transfer mechanics through the transition region are shown to result in additional rotations of the cross sections at the crack tip which in this study are captured through rotary and Timoshenko shear springs.

For example, as shown in Fig. 7, the right edge of "Transition Region" 1 is subjected to force and moment resultants N_1, V_1, M_1, which can be calculated in terms of N_t, V_t, M_t as discussed above. Meanwhile, the left edge of the transition region at cross section A located at a distance λa from the left crack tip ought to be subjected to either the deformation or traction conditions obtained through the beam bending theory as shown in Fig. 7. The force and moment resultants acting on the left edge of the transition region can thus be calculated using the normal and shear stress profiles at Section A as follows (see Fig. 7).

$$N_A^t = w \int_{y=\left(\frac{h}{2}-h_t\right)}^{y=\frac{h}{2}} \sigma_x(y)dy = -\frac{M_A}{2I}(h-h_t)wh_t\,, \tag{9a}$$

$$V_A^t = w \int_{y=\left(\frac{h}{2}-h_t\right)}^{y=\frac{h}{2}} \tau_{xy}(y)dy = -\frac{V_A I_t}{2I}\left(6\frac{h}{h_t}-4\right), \tag{9b}$$

$$M_A^t = w \int_{y=\left(\frac{h}{2}-h_t\right)}^{y=\frac{h}{2}} y\sigma_x(y)dy = \frac{I_t}{I}M_A\,. \tag{9c}$$

When comparing the above results to those given by Eqns (3), (5) and (7), one realizes that appreciable gradients in the axial, shear and bending moment resultants must exist in the transition region. For example, the bending moment at A can be expressed in terms of the bending moment at the crack center location M_C, the applied force P and the distance from the crack center (see Figs. 7 and 8) such that,

$$M_A = M_C - Pa(1+\lambda) \tag{10}$$

where as before M_C is the bending moment acting at the crack center location in the healthy beam;

P – is a downward transverse load as shown in Fig. 4;

a – is half the crack length;

λa – is the length of a transition region as shown in Figs. 7 and 8.

With the aid of Eqns (5), (7) and (9), one can show that

$$N_A^t - N_1 = M_C\left\{\frac{2}{h}\left(1-\frac{I_t}{I}-\frac{I_b}{I}\right)-\frac{h_t h_b}{2I}\right\}+6P\frac{a}{h}(1+\lambda)\frac{h_t}{h}\frac{h_b}{h} \text{ and}$$
$$M_A^t - M_1 = -Pa(1+\lambda)\frac{I_t}{I}+V_t a \tag{11}$$

In the case when the horizontal crack is located on the mid-plane of the healthy beam, i.e., $h_t = h_b = h/2$ it can be shown that $V_t = V_b = P/2$ and thus the axial force and bending moment differences between the quantities at cross section A and Interface 1 are calculated through Eqn. (11) to be,

$$N_A^t - N_1 = \frac{3}{2} P \frac{a}{h}(1+\lambda) \text{ and } M_A^t - M_1 = \frac{Pa}{8}(3-\lambda) \quad (12)$$

In the case of $\lambda \to 0$, the above equations suggest that both the force and moment resultants transferred through the mid-plane of the beams above and below the crack plane would exhibit inadmissible discontinuities in the absence of any external load changes. In fact, in accordance with Eqn. (12) under the condition of $\lambda = 0$, i.e., absence of any transition region, the force and moment discontinuities also shown schematically in Fig. 7, are predicted to be $N_A^t - N_1 = 3Pa/2h$ and $M_A^t - M_1 = 3Pa/8$. These findings form the foundation for the introduction of the transition regions shown in Figs. 7-9.

While the presence of the transition regions would allow the smooth transition of the force and moment resultants from the healthy beam response at section A to the cracked beam mechanics predicted in the crack region, their presence also has a profound effect on the deformation and fracture mechanics of the cracked beam.

In order to better understand the effects of the transition region on the overall beam deformation mechanics, let's consider the axial force and bending moment profiles presented in Fig. 7. The bottom half of the above figure shows a section of the beam in the crack region above the neutral axis of the healthy structure. It includes the left half of the top beam above the crack, or Beam-2 as well as its adjacent transition region labeled as "Transition Region 1". The transition region is of length λa with a being the half crack length. At Interface 1, the resultant forces and moment applied at the mid-plane of the top beam are N_1, V_1 and M_1. At the left edge of Transition Region 1, the resultant forces and moment N_A^t, V_A^t and M_A^t are obtained with the aid of Eqn. (9). Profiles of the axial force and bending moment predicted by Eqns (9) through (12) are sketched on the top half of Fig. 7. The profiles shown in solid black lines are predicted using Eqn. (9) for the healthy beam whereas the solid blue line profiles are those obtained with the aid of Eqns (3) through (7) for the crack region. As shown, at Interface 1, the moment and axial force predicted at the left edge of Transition Region 1, i.e., as $\lambda \to 0$, do not match those predicted by the crack beam model at Interface 1. As discussed earlier, the existence of the transition region is required for the smooth force and moment transition between Section A and Interface 1.

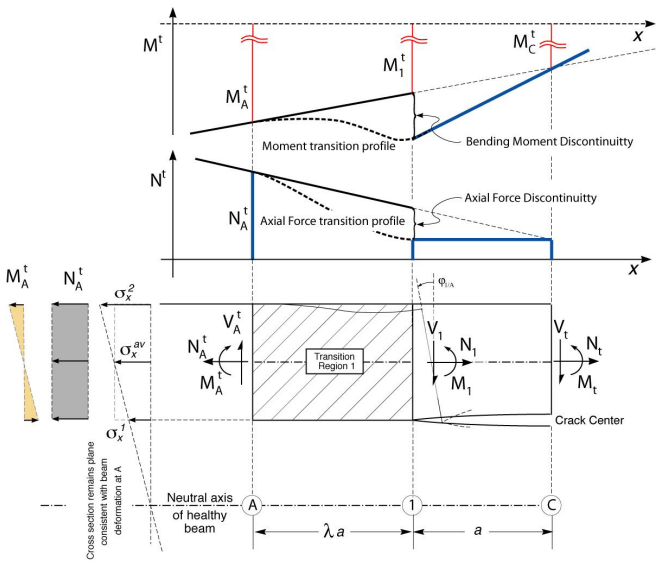

Fig. 7. Schematics showing the profiles of the bending moment and axial force transmitted through the mid-plane of the beam region above the crack plane. The linear profiles on the top left are consistent with the beam theory for the "healthy" beam. The heavy blue lines on the top right represent the profiles predicted by the model developed in this study (see Eqns (3) and (5)). The two results do not match at interface 1 leading to the conclusion that transient profiles are required for the smooth transition between the two profiles. In this study it is postulated that the discrepancy between the two profiles leads to the development of "extra rotations" in the transition region accounted for through rotary springs employed in this study.

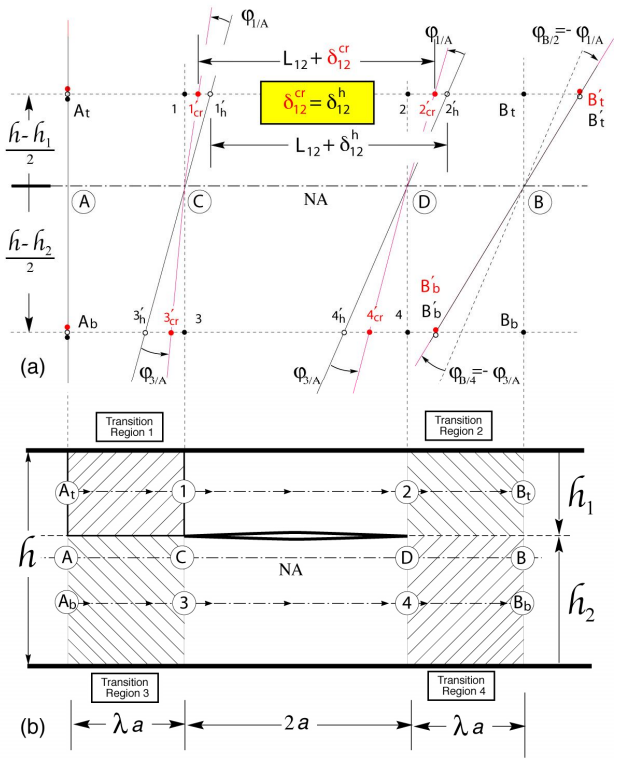

Fig. 8. Schematics showing the relative axial deformations and cross sectional rotations of reference points along the mid-planes of the "top" and "bottom" beams including their adjacent transition regions. Points $A_t \rightarrow 1 \rightarrow 2 \rightarrow B_t$ shown in (b) deformed to locations $A_t \rightarrow 1'_h \rightarrow 2'_h \rightarrow B'_t$ in the "healthy" beam whereas in the "cracked" beam they deformed to locations $A_t \rightarrow 1'_{cr} \rightarrow 2'_{cr} \rightarrow B'_{cr}$ as shown in (a). Similarly, points $A_b \rightarrow 3 \rightarrow 4 \rightarrow B_b$ deformed to $A_b \rightarrow 3'_h \rightarrow 4'_h \rightarrow B'_b$ in the "healthy" and to $A_b \rightarrow 3'_{cr} \rightarrow 4'_{cr} \rightarrow B'_b$ in the "cracked" beams respectively. The above schematics also highlights the accumulation of "extra" rotations $\varphi_{1/A}$ and $\varphi_{3/A}$ in the left transition regions which are offset by "extra rotations" $\varphi_{B/2}$ and $\varphi_{B/4}$ in the right transition regions.

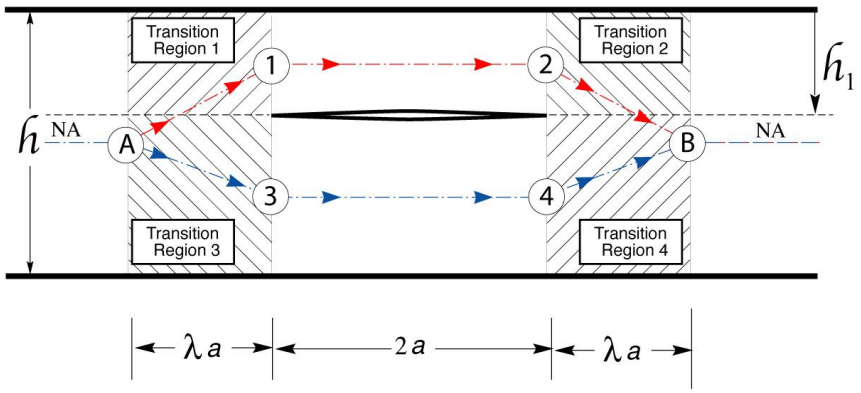

Fig. 9. The compatibility paths followed through the "top" and "bottom" beams in establishing angle of rotation and deflection compatibility conditions from reference section A to reference section B. Also shown are Transition Regions 1-4.

It is reasonable to assume that both the force and moment transitional profiles would be of the general type shown by the transitional profiles in dash black lines in Fig. 7. Under such conditions, reduction in both the force and moment resultants relative to the healthy beam, would result in lower axial strains along the mid-plane of the transition region and thus a comparatively lower extension of the transition region mid-plane relative to its healthy counterpart. This would appear in the cracked beam as a change in the rotary compliance giving rise to an additional angle of rotation $\varphi_{1/A}$ at Interface 1 as shown schematically in Figs. 7 and 8. A similar load transfer and deformation mechanism would exist in Transition Region 3 connecting Section A to the left end of the bottom beam at Interface 3. However, the axial force in the bottom beam being the opposite of that dominating the top beam would result in an added rotation in the same sense as that for Interface 1. The actual amount of added rotations should depend on the extent and thickness of the transition region and should be proportional to the cross sectional resultants N_1, V_1 and M_1. Since the axial force $N_1 = N_t$ with N_t linearly depending on M_t through Eqn. (5), while M_1 and M_t are linearly related through V_t and a in Eqn. (7), the following rotary and shear deformation equations are proposed for each transition region,

$$\varphi_{1/A} = \frac{M_1 \lambda a}{\kappa_1^m EI_t} \quad \text{and} \quad \delta_{1/A} = \frac{V_1 \lambda a}{k_t GA_t} \quad \textit{For Transition Region 1} \tag{13a}$$

$$\varphi_{2/B} = \frac{M_2 \lambda a}{\kappa_1^m EI_t} \quad \text{and} \quad \delta_{2/B} = \frac{V_2 \lambda a}{k_t GA_t} \quad \textit{For Transition Region 2} \tag{13b}$$

$$\varphi_{3/A} = \frac{M_3 \lambda a}{\kappa_3^m EI_b} \quad \text{and} \quad \delta_{1/A} = \frac{V_3 \lambda a}{k_b GA_b} \quad \textit{For Transition Region 3} \tag{13c}$$

$$\varphi_{4/B} = \frac{M_4 \lambda a}{\kappa_3^m EI_b} \quad \text{and} \quad \delta_{2/B} = \frac{V_4 \lambda a}{k_b GA_b} \quad \textit{For Transition Region 4} \tag{13d}$$

where κ_1^m and κ_3^m are the normalized rotary spring stiffness constants to be determined through compatibility conditions;

k_t and k_b are Timoshenko shear constants for the top and bottom beams respectively.

In postulating the above relations, it was assumed that the rotary and shear spring constants for Interfaces 1 and 2 are the same as well as those of Interfaces 3 and 4. It may be of importance to note that due to the anti-symmetry of the force and moment resultants jumps between Sections A and Interface 1 at the left crack tip and Interface 2 and Section B at the right crack tip as shown in Fig. 8, the added rotations capture by the above equations and occurring in Transition Region 1 would be offset by the added rotations at Interface 2 induced by the load and deformation mechanics in Transition Region 2. In fact, this observation has been validated using 2D finite elements and will be used as one of the compatibility conditions needed to determine the rotary and shear spring constants.

The above observation is further clarified with the aid of Figs. 8 and 9. In the above figures, emphasis is placed on the axial deformation of two reference lines, i.e., the mid-plane line segment of the top beam passing through the reference points $A_t \to 1 \to 2 \to B_t$ and its bottom beam counterpart passing through points $A_b \to 3 \to 4 \to B_b$. The red solid symbols represent the deformed position of the respective points in the cracked beam if the reference line was to stay straight whereas the open white symbols represent the corresponding deformed location of the same reference points in the healthy beam. In Fig. 8, all deformations are sketched relative to those at a reference cross section at A. For a downward applied load P the "beam" above the crack is subjected to tension whereas the one below the crack is subjected to compression. Consistent with the gradient force and moment profiles shown in Fig. 7 and discussed above, the line segment $A_t \to 1$ in Transition Region 1, would stretch less than its healthy beam counterpart. Thus the relative cracked beam and healthy beam deformed states are different as denoted by the $1'_{cr}$ and $1'_h$ positions with the latter being further to the right. Since no overall tension is applied to the beam structure, the neutral axis of the healthy beam would remain inextensible. When connecting the deformed reference points of the cracked beam and the healthy beam to their neutral axis counterpart a differential $\varphi_{1/A}$ angle of rotation is obtained when comparing the cracked and healthy beam systems. As discussed above, this rotation is postulated in this study to depend linearly on the cross sectional moment resultant M_1, the transition region length λa, while inversely proportional to an effective bending stiffness EI_t multiplied by a proportionality constant κ_1^m given by Eqn. (13a). Interestingly enough, a similar effect appears at Interface 3 through the compression and reduction of length arguments for line segment $A_b \to 3$ in Transition Region 3. In both instances, changes in the effective rotation of Interfaces 1 and 3 relative to the rotation of the healthy beam are predicted. At this stage, it is not apparent as to whether the predicted extra rotations $\varphi_{1/A}$ and $\varphi_{3/A}$ are related to each other and what that relationship is. As such, $\varphi_{3/A}$ is postulated to be proportional to the moment resultant M_3 at Interface 3 and inversely proportional to the effective bending stiffness $\kappa_3^m EI_b$.

While a differential rotation between the healthy and the cracked beam is predicted at Interfaces 1 and 3, it can be shown that the line segments $1 \to 2$ in the beam above the crack (top beam) and $3 \to 4$ in the beam below the crack (bottom beam) experience identical stretching or shrinkage in the cracked and healthy beams. This can be proven by integrating the axial strain $\varepsilon_x(x, y)$ along the respective paths in the cracked and healthy beams such that,

$$\int_{x=x_1}^{x=x_2} \varepsilon_x^{cr}\left(x, y = \tfrac{h-h_t}{2}\right) dx = \int_{x=x_1}^{x=x_2} \varepsilon_x^{h}\left(x, y = \tfrac{h-h_t}{2}\right) dx \tag{14}$$

In light of the above, the differential rotations between the cracked and healthy beam associated with Interfaces 1 and 3 remain as such at Interfaces 2 and 4. However, given the anti-symmetry of the force and moment resultant difference between the healthy and cracked beams relative to the crack

center, differential rotations take place in Transition Regions 2 and 4 in the opposite sense of those occurring in Transition Regions 1 and 3 fully offsetting one another at reference point B as suggested by the 2D Finite Element results reported elsewhere [33] and in Fig. 2. In this study, the transition crack lengths in all four transition regions are assumed to be equal while making the added rotations to be linearly dependent on the respective bending moment resultants as reflected by Eqn. (13). All rotary spring stiffness proportionality constants, i.e., κ_1^m and κ_3^m along with the transition region length parameter λ are to be determined through the compatibility conditions which shall be implemented next.

Compatibility of cross-sectional rotations. Cross sectional rotation and neutral axis deflection compatibility shall be enforced between Sections A and B following two separated paths along the top ($A \to 1 \to 2 \to B$) and bottom ($A \to 3 \to 4 \to B$) beams as shown in Fig. 9. More specifically, for compatibility purposes, it is required that,

$$\varphi_B = \varphi_A + \varphi_{1/A} + \varphi_{2/1} + \varphi_{B/2} = \varphi_A + \varphi_{3/A} + \varphi_{4/3} + \varphi_{B/4} \tag{15}$$

where φ_A and φ_B are the rotations of Sections A and B respectively while $\varphi_{1/A}$, $\varphi_{2/1}$ and $\varphi_{B/2}$ represent the relative rotations between Sections 1 and A, 2 and 1, and B and 2 respectively as shown schematically in Fig. 10.

The above equation is equivalent to state that ${\varphi^t}_{B/A} = {\varphi^b}_{B/A}$, or the change of the cross sectional rotation from A and B calculated through the mechanics of Transition Region 1, Beam-2 and Transition Region 2 should be identical to that calculated through the mechanics of Transition Region 3, Beam-3, and Transition Region 4. Thus, after eliminating φ_A appearing at both sides of Eqn. (15) the above compatibility equation simplifies to,

$$\varphi_{1/A} + \varphi_{2/1} + \varphi_{B/2} = \varphi_{3/A} + \varphi_{4/3} + \varphi_{B/4} \tag{16}$$

As discussed earlier in this study, when a Timoshenko beam is used, the rotational compatibility condition is imposed on the rotation of the cross section and not the slope of the beam consistent with Eqn. (8). The individual terms appearing in Eqn. (16) can be obtained using the postulated transition region equation (13) and the Timoshenko beam equation (8) as follows,

$$\varphi_{1/A} = \frac{M_1 \lambda a}{\kappa_1^m EI_t} \qquad \varphi_{3/A} = \frac{M_3 \lambda a}{\kappa_3^m EI_b}$$

$$\varphi_{2/1} = -\frac{V_2 (2a)^2}{2EI_t} + \frac{M_2 (2a)}{EI_t} \quad \text{and} \quad \varphi_{4/3} = -\frac{V_4 (2a)^2}{2EI_b} + \frac{M_4 (2a)}{EI_b}$$

$$\varphi_{B/2} = \frac{M_2 \lambda a}{\kappa_1^m EI_t} \qquad \varphi_{B/4} = \frac{M_4 \lambda a}{\kappa_3^m EI_b} \tag{17}$$

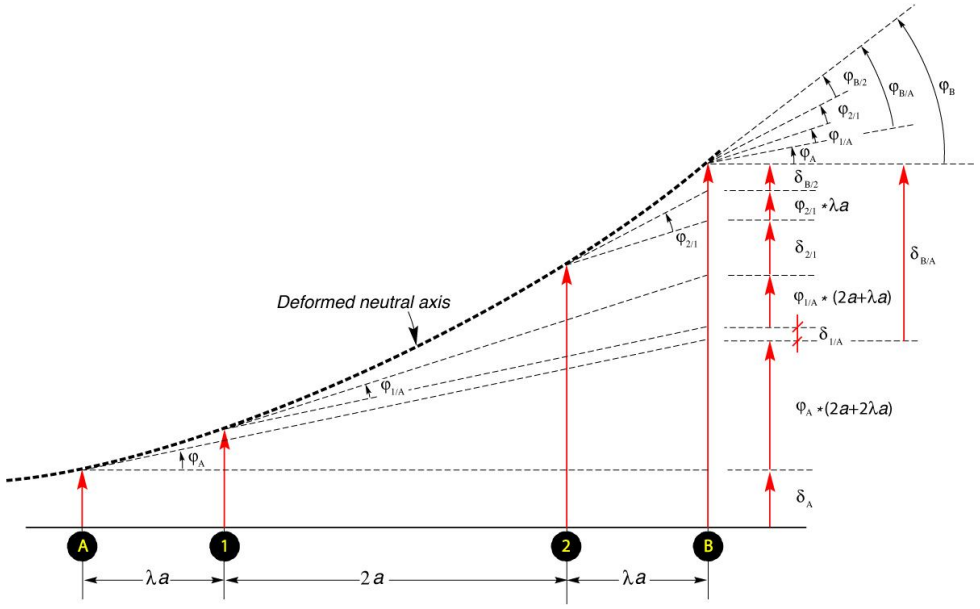

Fig. 10. The deformed neutral axis of a "continuous" beam from the reference cross section A to the reference cross section B highlighting the relations between cross sectional rotations and deflections along the compatibility path $A_t \rightarrow 1 \rightarrow 2 \rightarrow B_t$ shown in Figs. 8 and 9.

In the above equations, the assumption was made that $\kappa_1^m = \kappa_2^m$ and $\kappa_3^m = \kappa_4^m$. When substituting Eqn. (17) into (16), the following relationship is obtained,

$$\frac{M_t 2a}{EI_t}\left(\frac{\lambda}{\kappa_1^m}+1\right) = \frac{M_b 2a}{EI_b}\left(\frac{\lambda}{\kappa_3^m}+1\right) \tag{18}$$

Now utilizing Eqn. (2), i.e., $M_t / I_t = M_b / Ib = M_C / I$, the above relation yields,

$$\kappa_1^m = \kappa_3^m \tag{19}$$

Compatibility of deflections. Assisted by the deformation schematic shown in Fig. 10, the deflection at section B of the cracked beam can be obtained using the principle of linear superposition as follows,

$$\begin{aligned} &\delta_B = \delta_A + \delta_{1/A} + \varphi_{1/A}(2+\lambda)a + \delta_{2/1} + \varphi_{2/1}\lambda a + \delta_{B/2} \quad \text{using the } A\rightarrow 1 \rightarrow 2 \rightarrow B \text{ path} \\ &\qquad\qquad\qquad\qquad \text{or} \\ &\delta_B = \delta_A + \delta_{3/A} + \varphi_{3/A}(2+\lambda)a + \delta_{4/3} + \varphi_{4/3}\lambda a + \delta_{B/4} \quad \text{using the } A\rightarrow 3 \rightarrow 4 \rightarrow B \text{ path} \end{aligned} \tag{20}$$

The relative deflections $\delta_{1/A}, \delta_{3/A}, \delta_{B/2}$ and $\delta_{B/4}$ are related to the load transfer and deformation mechanics within the four transition regions. As discussed earlier in this work, the axial force and bending moment transition region effects lead to a postulated change in the angle of rotation at Interfaces 1 through 4. As such, the relative deflection due to shear in the same transition region

should be related to the application of the total resultant shear force which in the system under study equals the applied load P. Thus, the relative deflections at the mid-plane at Interfaces 1 and 3 at the left tip and Interfaces 2 and 4 at the right crack tip ought to be equal and most likely given by the Timoshenko shear term. In any case, since $\delta_{1/A} = \delta_{3/A}$ and $\delta_{B/2} = \delta_{B/4}$, the deflection compatibility condition must take the form,

$$\delta^t_{B/A} = \delta^b_{B/A} \tag{21}$$

which can be expressed as follows,

$$\varphi_{1/A}(\lambda+2)a + \delta_{2/1} + \varphi_{2/1}\lambda a = \varphi_{3/A}(\lambda+2)a + \delta_{4/3} + \varphi_{4/3}\lambda a \tag{22}$$

Again using the Timoshenko formulas given in Eqn. (8), the individual terms appearing in Eqn. (22) are given in terms of the cross sectional resultants and beam geometry and structural stiffnesses as follows,

$$\varphi_{1/A} = \frac{M_1 \lambda a}{\kappa_1^m EI_t} \qquad \varphi_{3/A} = \frac{M_3 \lambda a}{\kappa_3^m EI_b}$$

$$\delta_{2/1} = -\frac{V_2(2a)^3}{3EI_t} + \frac{M_2(2a)^2}{2EI_t} - \frac{V_1 2a}{k_t GA_t} \quad \text{and} \quad \delta_{2/1} = -\frac{V_4(2a)^3}{3EI_b} + \frac{M_4(2a)^2}{2EI_b} - \frac{V_4 2a}{k_b GA_b} \tag{23}$$

$$\varphi_{2/1} = -\frac{V_2(2a)^2}{2EI_t} + \frac{M_2(2a)}{EI_t} \qquad \varphi_{2/1} = -\frac{V_4(2a)^2}{2EI_b} + \frac{M_4(2a)}{EI_b}$$

where k_t and k_b – are the Timoshenko constants for Beam-2 and Beam-3 respectively.

By substituting the rotations and deflections given by Eqn. (23) into their respective equivalents in (22) and by making use the moment relations given in Eqn. (7), we arrive at the following deflection compatibility equation,

$$\frac{M_t a^2}{EI_t}\left[\frac{1}{\kappa_1^m}\lambda(2+\lambda) + 2(1+\lambda)\right] - \frac{V_t a^3}{EI_t}\left[\frac{1}{\kappa_1^m}\lambda(2+\lambda) + \frac{2}{3}\right] - \frac{V_t 2a}{k_t GA_t} = \tag{24}$$

$$= \frac{M_b a^2}{EI_b}\left[\frac{1}{\kappa_3^m}\lambda(2+\lambda) + 2(1+\lambda)\right] - \frac{V_b a^3}{EI_b}\left[\frac{1}{\kappa_3^m}\lambda(2+\lambda) + \frac{2}{3}\right] - \frac{V_b 2a}{k_b GA_b}$$

It has already been established that $\kappa_1^m = \kappa_3^m$ (see Eqn. (19)), and given the fact that $M_t / I_t = M_b / Ib = M_C / I$, the above equation further simplifies to the following shear force ratio equation.

$$\frac{V_t}{V_b}=\frac{I_t}{I_b}\frac{\frac{1}{\kappa_1^m}\lambda(2+\lambda)+2(1+\lambda)+\frac{2}{k_b}\frac{I_b}{A_b a^2}\frac{E}{G}}{\frac{1}{\kappa_1^m}\lambda(2+\lambda)+2(1+\lambda)+\frac{2}{k_t}\frac{I_t}{A_t a^2}\frac{E}{G}} \tag{25}$$

It is obvious that in order to establish the above shear force ratio, κ_1^m and λ need to be determined through additional conditions as will be discussed below. However, it is worth noting that when ignoring the Timoshenko shear effects, i.e., letting k_t and $k_b \to \infty$, then the following simple form for the shear force ratio is obtained,

$$\frac{V_t}{V_b}=\frac{I_t}{I_b} \tag{26}$$

It is also noteworthy to observe for systems in which the crack is on the beam neutral axis (i.e., $h_1 = h_2$), both Eqns. (25) and (26) predict that the shear force ratio between the shear resultants in the top and bottom beam is $V_t/V_b = 1$ and thus from the global equilibrium enforced by Eqn. (6), it can be shown that $V_t = V_b = P/2$. As will be discussed later, shear force predictions obtained by the present model were found to compare very well with 2D finite element results.

Calculating the normalized rotary spring stiffness. Of the two remaining unknowns, i.e., κ_1^m and λ, the normalized rotary spring stiffness κ_1^mcan be estimated using the second key observation from 2D finite elements (see Fig. 2), i.e., *the neutral axis rotation (slope) of the cracked beam in the region between the applied load and the nearest crack tip matches the corresponding slope of the healthy beam.* The above observation leads to the following condition,

$$\varphi^{cr}{}_{B/A}=\varphi^{h}{}_{B/A} \tag{27}$$

where the superscripts $)^{cr}$ and $)^{h}$ denote quantities for the cracked and healthy beams respectively. The left hand side of the above equation is equal to the left hand side of Eqn. (18). Thus, the above relation can be written in terms of the moment and shear force resultants as follows,

$$\varphi^{cr}{}_{B/A}=\frac{M_t 2a}{EI_t}\left(\frac{\lambda}{\kappa_1^m}+1\right)=\varphi^{h}{}_{B/A}=-\frac{V_B(2a(1+\lambda))^2}{2EI}+\frac{M_B 2a(1+\lambda)}{EI} \tag{28}$$

where $V_B = P$ and $M_B = M_C + Pa(1+\lambda)$.

In light of the above, Eqn. (28) above takes the form,

$$\frac{M_t 2a}{EI_t}\left(\frac{\lambda}{\kappa_1^m}+1\right)=\frac{M_C 2a}{EI}(1+\lambda) \tag{29}$$

Again utilizing Eqn. (2), i.e., $M_t / I_t = M_b / Ib = M_C / I$, the above equation reduces to

$$\frac{M_C 2a}{EI}\left(\frac{\lambda}{\kappa_1^m} - \lambda\right) = 0 \quad \text{which leads to} \quad \kappa_1^m = 1 \tag{30}$$

The above finding along with Eqn. (19) suggest that $\kappa_1^m = \kappa_3^m = 1$ and thus the rotary spring stiffnesses are as follows,

$$\begin{aligned} \kappa_1 &= M_1 / \varphi_{1/A} = EI_t / \lambda a, \quad \kappa_2 = M_2 / \varphi_{B/2} = EI_t / \lambda a \\ \kappa_3 &= M_3 / \varphi_{3/A} = EI_b / \lambda a, \quad \kappa_4 = M_4 / \varphi_{B/4} = EI_b / \lambda a \end{aligned} \tag{31}$$

where λa is the extent of the transition regions to be determined next.

On the transition region. The above findings reflected through Eqn. (31), highlight the importance of the transition regions in understanding the load transfer and deformation mechanics in a beam with a horizontal sharp crack. The postulated rotations at Interfaces 1 through 4 at the left and right crack tips are found to depend on the extent or length of the transition region λa. Thus, the full development of the four-beam model proposed in this study requires the determination of the transition region length λa. As will be presented later on in this section, in this study we make use of an independent beam deflection estimate at the free end obtained numerically via the method of finite elements. Thus by matching the beam deflection estimated through the beam model to that obtained through finite elements, a non-linear equation in λ is obtained through which estimates for the normalized transition region length. However, before developing the consistency equation in λ, it may be of value to this and subsequent studies to consider the load transfer and deformation mechanics in the transition regions. For example, let us consider the mechanics of Transition Region 1, shown in Fig. 11. As shown in the above figure, on the left edge of the above transition region, the force and moment resultants would be those obtained from the bending theory consistent with Eqn. (9) as discussed earlier. On the right edge, different moment and force resultants are applied consistent with the mechanics of the cracked beam presented earlier in this study. As discussed earlier, the rotary beam changes relative to the healthy.

can be attributed to the load transfer through the transition region in which the resultants obtained on the left edge must transition to the resultants estimated for the right edge. At this point one has to also account for the singular stress field dominating the crack tip region. For example, based on the crack tip region reference system x', y' shown in Fig. 11, the normal stress $\sigma_x(y)$ acting on the vertical interface 1 in the crack tip region can be obtained by evaluating the respective crack tip stress at $\theta' = -90^o$, i.e.,

$$\sigma_x(y) = \sigma_{x'}\left(r', \theta' = -\frac{\pi}{2}\right) = \frac{K_I}{\sqrt{2\pi r}}\cos\left(\frac{\theta'}{2}\right)\left(1 - \sin\left(\frac{\theta'}{2}\right)\sin\left(\frac{3\theta'}{2}\right)\right)_{\theta'=-\frac{\pi}{2}}$$

$$+\frac{K_{II}}{\sqrt{2\pi r}}\left(-sin(\tfrac{\theta'}{2})\right)\left(2 + \cos(\tfrac{\theta'}{2})\cos(\tfrac{3\theta'}{2})\right)_{\theta'=-\frac{\pi}{2}} = \frac{1}{4\sqrt{\pi}}(K_I + 3K_{II})y^{-1/2} \tag{32}$$

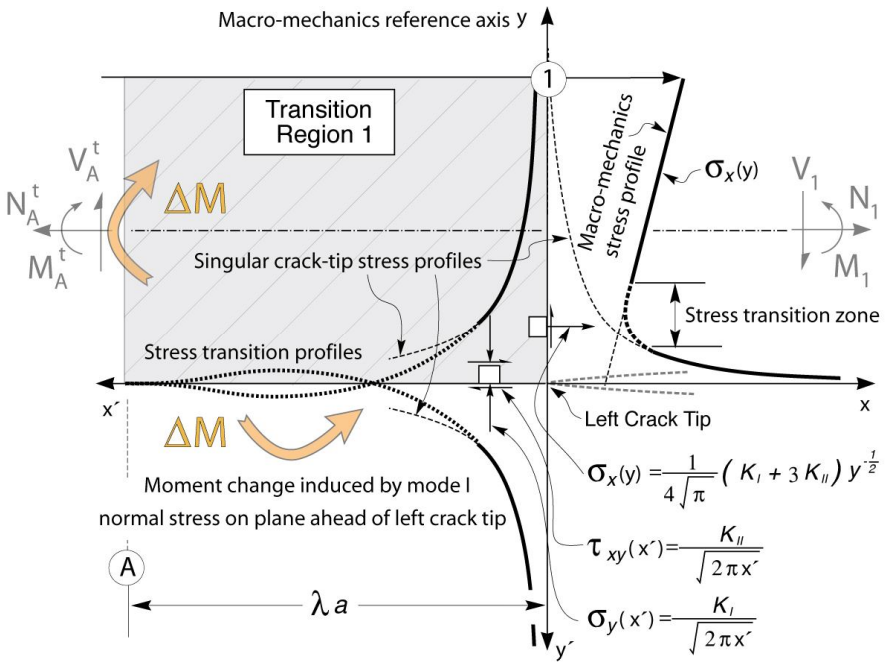

Fig. 11. Schematics of potential transition region stress fields that are superimposed onto those of the healthy beam. These fields are shown to conform to the near-tip mixed mode fields near the crack tip region and to the macro-mechanical field differences sufficiently away from the crack tip. As shown, a change of moment ΔM is induced by the mode I component of the stress intensity factor on the crack plane ahead of the left crack tip. An equal and opposite moment change then must occur on the left vertical plane of the transition region thus causing a slight "bump" on the moment and associated curvature profile at the start of the transition region as shown in Fig. 3.

The above singular stress profile is shown in Fig. 11 with a heavy solid line in the proximity of the crack tip continuing with a light dash line away from the singular region. Meanwhile, sufficiently away from the crack tip region, the same stress component must follow the linear mechanics of material profile predicted by the system macro mechanics. As shown in Fig. 11, a stress transition region must also exist as needed for the smooth transition of the $\sigma_x(y)$ component between the two fields. It is reasonable to expect that such a stress profile that accounts for both the finite macro mechanics profile as well as the singular near-tip profile would cause a shift of the plane on which the force resultant is effectively acting. A similar argument can be made for the shear stress acting on the same vertical plane (i.e., Interface 1) as well as for the normal $\sigma_x(y)$ and shear $\tau_{xy}(x)$ profiles acting on the horizontal transition region edge ahead of the crack tip. Such observations would naturally lead to the conclusion that a rather convoluted stress field dominates the transition region and that it's structure and intensity should also depend on the stress intensity factors K_I, K_{II} associated with the related crack tip. With this in mind, it is expected that the extent of the transition region λa should include information related to the crack-tip domain and thus could depend on the structure of the mixed mode [40-45] singular fields and possibly the magnitude of the related stress intensity factor.

Another relevant observation is that the presence of even a slight mode I component would induce a tensile normal stress if $K_I > 0$ associated with crack tip opening, or compressive if $K_I < 0$ associated with crack surface contact as shown schematically in Fig. 11. The presence of such a stress close to the crack tip will need to be offset by an opposite stress resultant away from the crack tip in the transition region. Such a stress profile would then induce a net moment ΔM on the plane ahead of the crack tip in the transition region which ought to be counter-balanced by an equal and opposite moment on the vertical left edge of the transition region. Such a moment change could explain the free surface curvature "bump" observed via finite elements as shown in Fig. 3. Thus, the presence of

such a curvature "bump" could indicate the existence of crack damage in the vicinity of such a measurement used in non-model damage detection methods [46-49].

Given the above qualitative considerations regarding the mechanics of the transition region, several methods can be employed in calculating the relationship between λ and the various problem variables that may affect the local stress intensities. One such method is to evaluate the crack-tip stress intensities and or associated energy release rate using either a compliance method [28-31, 50] or a J-integral approach [40] based on the model findings of this study. Those estimates can then be compared to independent estimates obtained for example using the method of finite elements which will then yield a consistency equation in λ. Yet, another possible approach is to extract the transition domain and conduct rigorous numerical and possibly theoretical studies in solving the requisite boundary value problem thus required to establish the load transfer and deformation mechanics of the transition region. Such an approach would allow for parametric studies needed to establish the relative deformation of the right edge of the transition region relative to the left. Such estimates would be used in determining the differential deformation between the cracked and healthy structures thus giving estimates of the rotary changes induced by the introduction of the crack and thus obtained estimates of the rotary spring stiffnesses which can then be used to obtain the transition length constant λ through Eqn. (31). Such studies are currently being pursuit which are expected to be presented in future works. In this work however, we employ a beam deflection matching alternative in determining the transition length constant λ as discussed below.

Beam deflection matching. The global mechanics of a beam with a crack includes the effects of the crack tip regions. Thus, the beam deformations anywhere in its domain including the deflection at its free end include the effects of the dominant stress intensity factors at both crack tips. Thus, one can use a known solution obtained by any other method including experimental techniques and numerical approaches such as the method of finite elements, to calibrate the four-beam model developed in this study as an effective way to calculating the transition length constant λ.

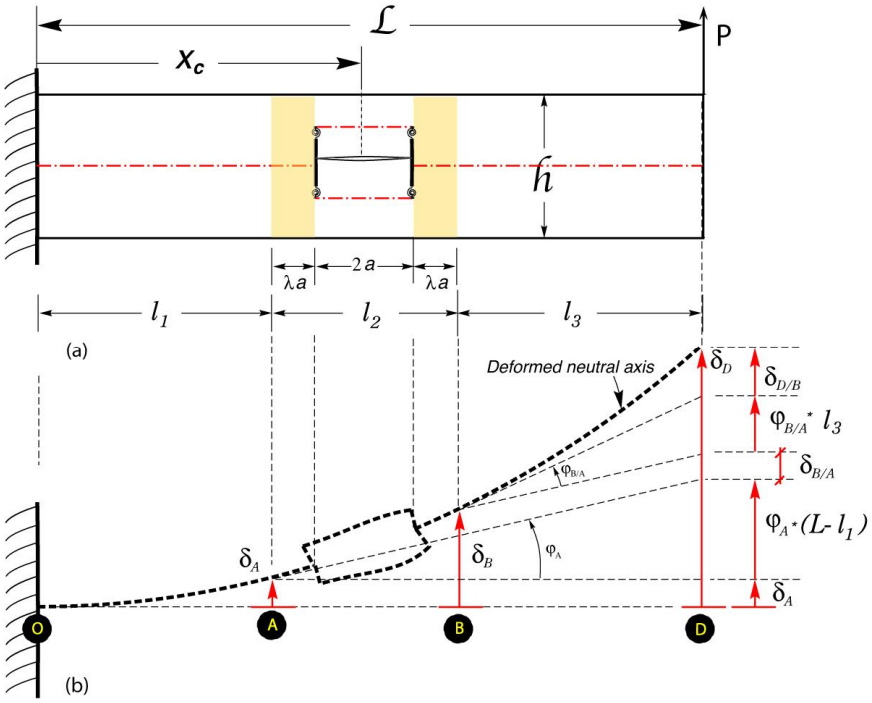

Fig. 12. A schematics showing (a) the original cracked beam with its un-deformed neutral axis and (b) the deformed neutral axis configuration of the four beam model. The relationship between the deflections and rotations at key reference points of the beam are also shown in (b). The deformations and rotations between Sections A and B include the transition region effects captured by the rotary spring and Timoshenko shear effects.

With the aid of Fig. 12, the deflection of the beam at its free end at D is given by,

$$\delta_D = \delta_A + \varphi_A(L - I_1) + \delta_{B/A} + \varphi_{B/A} I_3 + \delta_{D/B} \tag{33}$$

where $\delta_{B/A}$ and φ_A – are the deflection and angle of rotation at the cross section A at the start of the transition region at the left crack tip;

$\delta_{B/A}$ and $\varphi_{B/A}$ – are the deflection and angle of rotation respectively of Section B at the end of the transition region at the right crack tip relative to A;

and $\delta_{D/B}$ – is the deflection of the free end at D relative to B.

It is important to note that in this analysis, the effects of the transition regions are included in the relative terms $\delta_{B/A}$ and $\varphi_{B/A}$, and thus do not appear directly in Eqn. (33) above. Using the Timoshenko formulas for the deflection and rotations of a cantilever beam given in Eqn. (8) along with the outcomes on the relative deformations of Section B relative to A used earlier in this study the individual terms appearing in Eqn. (33) take the form,

$$\delta_A = -\frac{Pl_1^3}{3EI} - \frac{P(L-l_1)l_1^2}{2EI} - \frac{Pl_1}{kGA} \text{ and } \varphi_A = -\frac{Pl_1^2}{2EI} - \frac{P(L-l_1)l_1}{EI} \tag{34a}$$

$$\delta_{B/A} = \frac{M_t a^2}{EI_t}\left[\frac{1}{\kappa_1^m}\lambda(2+\lambda) + 2(1+\lambda)\right] - \frac{V_t a^3}{EI_t}\left[\frac{1}{\kappa_1^m}\lambda(2+\lambda) + \frac{2}{3}\right] - \frac{V_t 2a}{k_t G A_t} - \frac{P2\lambda a}{kGA} \tag{34b}$$

$$\varphi_{B/A} = \frac{M_t 2a}{EI_t}\left(\frac{\lambda}{\kappa_1^m} + 1\right) \tag{34c}$$

$$\delta_{D/B} = -\frac{Pl_3^3}{3EI} - \frac{Pl_3}{kGA} \tag{34d}$$

where $l_1 = x_C - a(1+\lambda)$, $l_2 = 2a(1+\lambda)$, $l_3 = L - \left(x_C + a(1+\lambda)\right)$, $M_t/I_t = M_C/I$, and $M_C = -P(L - x_C)$. Also in the above formulas, $\kappa_1^m = 1$ consistent with Eqn. (30) while V_t can be expressed in terms of the load P and the shear force ratio V_t/V_b given by Eqn. (25). Furthermore, in Eqn. (34), the constants k and k_t are the Timoshenko shear constants for the healthy beam and Beam-2 above the crack respectively. Thus using the above equations and after normalizing each term with respect to a characteristic deflection $\Delta = PL^3/E'I$, the following consistency condition in which the only unknown is the transition region length constant λ is obtained,

$$\delta_D = -\frac{PL^3}{E'I}\left\{\hat{\delta}_A + \hat{\varphi}_A(1-\hat{l}_1) + \hat{\delta}_{B/A} + \hat{\varphi}_{B/A}\hat{l}_3 + \hat{\delta}_{D/B}\right\} = -\frac{PL^3}{EI}\left\{\frac{1}{12}\left(\frac{h}{L}\right)^3 \hat{\delta}^{FE}{}_D\right\} \tag{35}$$

Where the $\hat{}$ symbol denotes normalized quantities with all length quantities normalized with respect to the beam length L and $E' = E/(1-\nu^2)$ is used to convert the beam plane stress to its plane strain equivalent solution. Also in the above consistency equation, $\hat{\delta}_D^{FE}$ is the absolute value of the deflection of the cracked beam at its free end obtained through non-dimensional FE simulations as

will be discussed later in the study. In light of the above normalization, the following expanded form of the consistency equation in λ is obtained,

$$\delta_D^{MM} = -\frac{(1-\nu^2)PL^3}{EI}\left\{\frac{1}{3}\hat{l}_1^3 + \frac{1}{2}(1-\hat{l}_1)\hat{l}_1^2 + \frac{(\hat{l}_1+\hat{l}_3)(1+\nu)}{6k}\left(\frac{h}{L}\right)^2 + \left(\frac{1}{2}\hat{l}_1^2 + (1-\hat{l}_1)\hat{l}_1\right)(1-\hat{l}_1)\right.$$

$$+(1-\hat{x}_C)\hat{a}^2(2+4\lambda+\lambda^2) + \frac{V_t}{P}\frac{I}{I_t}\hat{a}^3\left(\frac{2}{3}+\lambda(2+\lambda)\right) + \frac{V_t}{P}\frac{\hat{a}(1+\nu)}{3k_t}\left(\frac{h}{L}\right)^2\frac{h}{h_1} \tag{36}$$

$$\left.+\frac{\lambda\hat{a}(1+\nu)}{6k}\left(\frac{h}{L}\right)^2 + (1-\hat{x}_C)2\hat{a}(1+\lambda)\hat{l}_3 + \frac{1}{3}\hat{l}_3^3 = -\frac{PL^3}{EI}\left\{\frac{1}{12}\left(\frac{h}{L}\right)^3\hat{\delta}^{FE}{}_D\right\}\right.$$

As established earlier (see Eqn. (25), the shear force ratio can be expressed as follows,

$$\frac{V_t}{V_b} = \frac{I_t}{I_b}\gamma(\lambda) \tag{37}$$

where

$$\gamma(\lambda) = \frac{2+4\lambda+\lambda^2+\dfrac{(1+\nu)}{3k_b}\left(\dfrac{h_2}{a}\right)^2}{2+4\lambda+\lambda^2+\dfrac{(1+\nu)}{3k_t}\left(\dfrac{h_1}{a}\right)^2} \tag{38}$$

Clearly, when $h_1 = h_2$, and the Timoshenko constants $k_t = k_b$, the factor $\gamma = 1$ and thus $V_t/V_b = 1$ which yields $V_t/P = 1/2$. It is also worth noting that when ignoring the Timoshenko shear effects, i.e., $k_t, k_b \to \infty$, then $\gamma = 1$ and the ratio V_t/V_b and thus V_t/P become independent of λ. Regardless, the consistency equation given by (36) takes on the following form in λ,

$$\alpha(\lambda)\lambda^2 + \beta(\lambda)\lambda + \eta(\lambda) = 0 \tag{39}$$

where the equation coefficients are functions of λ either explicitly as shown below or implicitly through the beam lengths $\hat{l}_1(\lambda)$, $\hat{l}_2(\lambda)$, $\hat{l}_2(\lambda)$ and are given by,

$$\alpha(\lambda) = (1-\hat{x}_C)\hat{a}^2 + \frac{\gamma I}{I_b+\gamma I_t}\hat{a}^3,$$

$$\beta(\lambda) = 4(1-\hat{x}_C)\hat{a}^2 + 2\frac{\gamma I}{I_b+\gamma I_t}\hat{a}^3 + 2(1-\hat{x}_C)\hat{a}\hat{l}_3 + \frac{\hat{a}(1+\nu)}{6k}\left(\frac{h}{L}\right)^2,$$

$$\eta(\lambda)=\frac{1}{3}(\hat{l}_1^3+\hat{l}_3^3)+(1-\hat{l}_1)\hat{l}_1^2+\hat{l}_1(1-\hat{l}_1)^2+2\hat{a}(1-\hat{x}_C)(\hat{a}+\hat{l}_3)$$

$$+\frac{V_t}{P}\left[\frac{2}{3}\frac{I}{I_t}\hat{a}^3+\frac{(1+\nu)\hat{a}}{3k_t}\left(\frac{h}{L}\right)^2\frac{h}{h_1}\right]+\frac{(1+\nu)(\hat{l}_1+\hat{l}_3)}{6k}\left(\frac{h}{L}\right)^2 \tag{40}$$

$$-\frac{1}{12(1-\nu^2)}\left(\frac{h}{L}\right)^3\hat{\delta}_D^{FE}$$

In the above equation, the finite element term is divided by the $(1-\nu^2)$ factor as needed to match the beam plane stress and the 2D FE plane strain solutions. The above consistency equation in λ will be solved for several cases wherein the horizontal crack is placed at different locations along the length and height of the beam. However, in order to carry out this task, finite element solutions for the non-dimensional deflection of the beam at the free end will need to be obtained. Thus, a brief description of the finite element models used in these simulations would be discussed in the second part, i.e., Part B of this report.

Summary. This study represents the first part of a two-part study aimed at modeling the mechanical response of a cantilever beam containing an embedded horizontal crack and subjected to end transverse force condition. Informed by 2D finite element findings reported elsewhere [33] and summarized in this work, a four-beam mechanics of materials model has been developed capable of predicting the load transfer and deformation mechanics of a cracked cantilever beam discussed above. The model employs the transition regions associated with four rotary springs as a means of accounting for the load transfer through the regions adjacent to the crack tips. The rotary springs account for relative cross sectional rotations in the transition region induced by changes in the axial force and bending moments through the crack region.

Initially, the load transfer through the crack region was addressed. Finite element observations reported elsewhere [33] of matching curvatures enabled the development of analytical models capable of predicting the bending moment and axial force transmitted through the beams above and below the crack. The above quantities were then incorporated into the four-beam model which was used to obtain estimates of the transition region length as well as estimates of the shear force distribution in the beams above and below the crack. Deflection and cross-sectional rotation compatibility conditions were used in establishing the effective rotary spring stiffnesses, which capture the effects of the transition region. The transition region length is obtained via non-linear equation derived by matching the free end deflection of the cracked beam predicted by the current model to independent estimates obtained via the method of finite elements. The finite element model formulation along with the results obtained through broad parametric studies and related discussion is presented in a Part-B companion paper.

References

[1] Thomson, T.W. & Dahleh, M.D. (1993). Theory of Vibration with Applications, 5th Ed. Prentice Hall.

[2] Stanbridge, A.B., Martarelli, M. & Ewins, D.J. (1999). Measuring Area Mode Shapes with a Scanning Laser Doppler Vibrometer. *Proceedings of International Modal Analysis Conference*, 1999, Kissimmee, FL.

[3] Ewins, D.J. (2000). Modal Testing: Theory, Practice and Application, 2nd edition. Research Studies Press Ltd., Baldock, Hertfordshire, England: 422-427. 37.

[4] Stanbridge, A.B., Ewins, D.J. & Khan, A.Z. (2000). Modal Testing Using Impact Excitation and a Scanning LDV. *Shock and Vibration*, *7*, 91-100.

[5] Vignola, J.F., Judge, J.A. & Kurdila, A.J. (2009). Shaping of a System's Frequency Response Using an Array of Subordinate Oscillators. *Journal of the Acoustical Society of America*, *126(1)*, 129-139.

[6] Rizos, P.F., Aspragathos, N. & Dimarogonas, A.D. (1990). Identification of Crack Locations and Magnitude in a Cantilever Beam from Vibration Modes. *J. of Sound and Vibration*, *138(3)*, 381-388.

[7] Wong, C.N., Zhu, W.D. & Xu, G.Y. (2004). On an Iterative General-Order Perturbation Method for Multiple Structural Damage Detection. *J. Sound and Vibration*, *273*, 363-386.

[8] Xu, G.Y., Zhu, W.D. & Emory, B.H. (2007). Experimental and Numerical Investigation of Structural Damage Detection Using Changes in Natural Frequencies. *J. Vibration and Acoustics*, *129(6)*, 686-700.

[9] He, K. & Zhu, W.D. (2011). A Vibration-based Structural Damage Detection Method and Its Applications to Engineering Structures. *International Journal of Smart and Nano Materials*, *2(3)*, 194-218, doi: 10.1080/19475411.2011.594105

[10] Xu, Y.F. & Zhu, W.D. (2011). Operational Modal Analysis of a Rectangular Plate Using Noncontact Acoustic Excitation. *Proceedings of the International Modal Analysis Conference*, 2011, Jacksonville, FL, doi: 10.1007/978-1-4419-9428-8_30

[11] He, K. & Zhu, W.D. (2010). Detection of Damage and Loosening of Bolted Joints in Structures Using Changes in Natural Frequencies. *ASNT Material Evaluation*, June, 2010, 721-732, doi: 10.1088/1742-6596/305/1/012054

[12] He, K. & Zhu, W.D. (2011). Damage Detection of Space Frame Structures with L-shaped Beams and Bolted Joints Using Changes in Natural Frequencies. *Proceedings of the 23rd ASME Biennial Conference on Mechanical Vibration and Noise*, Washington, DC, Aug. 28-31, 2011, doi:10.1115/DETC2011-48982

[13] He, K. & Zhu, W.D. (2011). Detecting Loosening of Bolted Connections in a Pipeline Using Changes in Natural Frequencies. *Proceedings of the 23rd ASME Biennial Conference on Mechanical Vibration and Noise*, Washington, DC, Aug. 28-31, 2011.

[14] He, K. & Zhu, W.D. (2011). Finite element modeling of structures with L-shaped beams and bolted joints. *ASME Journal of Vibration and Acoustics*, Vol. 133(1), doi:10.1115/1.4001840

[15] He, K. & Zhu, W.D. (2009). Modeling of Fillets in Thin-walled Beams Using Shell/Plate and Beam Finite Elements. *ASME Journal of Vibration and Acoustics*, *131*, 051002 (16 pages), doi:10.1115/1.3142879

[16] Lin, R.J. & Cheng, F.P. (2008). Multiple crack Identification of a Free-free Beam with Uniform Material Property Variation and Varied Noised Frequency. *Engineering Structures*, *30*, 909-929.

[17] Ganeriwala, S.N., Yang, J. & Richardson, M. (2011). Using Modal Analysis for Detecting Cracks in Wind Turbine Blades. *Sound and Vibration.*, *45(5)*, 10-13.

[18] Das, P. (2012). Detection of Cracks in Beam Structures Using Modal Analysis. *Applied Mechanics and Materials*, *105-107*, 689-694.

[19] Swamidas, A.S., Yang, X. & Seshadri, R. (2004). Identification of cracking in beam structures using Timoshenko and Euler formulations. *J. Eng. Mech., 130(11)*, 1297–1308.

[20] Caddemi, S. & Calio, I. (2009). Exact closed-form solution for the vibration modes of the Euler-Bernoulli Beam with multiple open cracks. *J. Sound and Vibration*, *327*, 473-489.

[21] Rubio, L. (2011). An Efficient Method for Crack Identification in Simply Supported Euler-Bernoulli Beams. *Journal of Vibrations and Acoustics*, *131*, 051001-1 to 051001-6.

[22] Krawczuk, M. & Ostachowicz, W.M. (1995). Modeling and Vibration Analysis of a Cantilever Composite Beam with a Transverse open crack. *J. Sound and Vibration, 183(1)*, 69-89.

[23] Dimarogonas, A.D. (1996). Vibration of Cracked Structures: A State of the Art Review. *Engineering Fracture Mechanics, 55(5)*, 831-857.

[24] Wang, K., Inman, D.J. & Farrar, C.R. (2005). Modeling and Analysis of a Cracked Composite Beam Vibrating in Coupled Bending and Torsion. *J. Sound and Vibration*, *284*, 23-49.

[25] Zhang, X.Q., Han, Q. & Li, F. (2010). Analytical Approach for Detection of Multiple Cracks in a Beam. *J. Eng. Mech.*, *136(3)*, 345-357.

[26] Chatterjee, A. (2011). Nonlinear Dynamics and Damage Assessment of a Cantilever Beam with Breathing Edge Crack. *J. Vibration and Acoustics, 133(5)*, 051004-1 to 051004-6, doi:10.1115/1.4003934

[27] Liu, J., Zhu, W.D., Charalambides, P.G., *et al.* (2016). Four-beam Model for Vibration Analysis of a Cantilever Beam with an Embedded Horizontal Crack. *Chinese Journal of Mechanical Engineering*, *29(1)*, 163-179. doi: 10.3901/CJME.2015.0901.108

[28] Broek, D. (1974). Elementary Engineering Fracture Mechanics. Springer Press.

[29] Kanninen, M.F. & Popelar, C.H. (1986). Advanced Fracture Mechanics. Oxford Press.

[30] Anderson, T.L. (1991). Fracture Mechanics: Fundamentals and Applications, Second Editions. CRC Press Inc.

[31] Data, H., Paris, P.C. & Irwin, G.R. (2000). The Stress Analysis of Cracks Handbook, 3rd Edition. American Society of Mechanical Engineers Press.

[32] Erdogan, E. (2000). Fracture Mechanics. *International Journal of Solids and Structures*, *27*, 171-183.

[33] Fang, X. (2013). The Mechanics of an Elastically Deforming Cantilever Beam with an Embedded Sharp Crack Subjected to an End Transverse Load. Ph.D. Dissertation. Department of Mechanical Engineering, The University of Maryland, Baltimore County. December 2013.

[34] Fang, X. & Charalambides, P.G. (2015). The Fracture Mechanics of Cantilever Beams with an Embedded Sharp Crack under End Force Loading. *Engineering Fracture Mechanics*, Vol. *149*, 1-17, doi:10.1016/j.engfracmech.2015.09.039

[35] Aladzyeu, V. (2013). The Dynamic Response of an Elastic Structure with an Embedded Sharp Crack for Damage Detection. Ph.D. Dissertation. Department of Mechanical Engineering, The University of Maryland, Baltimore County. December 2013.

[36] Sokolnikoff, I.S. (1956). Mathematical Theory of Elasticity, 2nd Edition. McGraw-Hill Press.

[37] Timoshenko, S.P. (1921). On the correction factor for shear of the differential equation for transverse vibrations of bars of uniform cross-section. Philosophical Magazine, p. 744.

[38] Cowper, G.R. (1966). The Shear Coefficient in Timoshenko's Beam Theory. *ASME*, *J. Appl. Mech.*, *33*, 335-340.

[39] Riley, W.F., Sturges, L.D. & Morris, D.H. (2008). Mechanics of Materials, Sixth Edition. John Wiley & Sons, Inc.

[40] Rice, J.R. (1968). A Path Independent Integral and the Approximate Analysis of Strain Concentration by Notches and Cracks. *J. Appl. Mech.*, *35*, 379-386.

[41] Rice, J.R. (1988). Elastic Fracture Mechanics Concepts for Interfacial Cracks. *J. Appl. Mech.*, *55*, 98-103.

[42] Charalambides, P.G. (1990). Fiber Debonding in Residually Stressed Brittle Matrix Composites. *J. Am. Ceram. Soc.*, *73(6)*, 1674-1680.

[43] Charalambides, P.G., Lund, J., Evans, A.G. & McMeeking, R.M. (1989). A Test Specimen for Determining the Fracture Resistance of Bimaterial Interfaces. *J. Appl. Mech.*, *56(1)*, 77-82.

[44] Charalambides, P.G. (1991). Steady-State Delamination Cracking in Laminated Ceramic Matrix Composites. *J. Am. Ceram. Soc.*, *74(12)*, 3066-3080.

[45] Hutchinson, J.W. & Suo, Z. (1992). Mixed-mode cracking in layered materials. *Advances in Applied Mechanics*, *29*, 63-191.

[46] Pandey, A.K., Biswas, M. & Samman, M.M. (1991). Damage Detection from Changes in Curvature Mode Shapes. *J. Sound and Vibration*, *145(2)*, 321-332.

[47] Ratcliffe, C.P. (2000). A Frequency and Curvature Based Experimental Method for Locating Damage in Structures. *J. Vibration and Acoustics*, *122(3)*, 324-329.

[48] Ratcliffe, C.P. & Crane, R.M. (2005). Structural Irregularity and Damage Evaluation Routine (SIDER) for Testing of the ½-Scale Corvette Hull Section Subjected to UNDEX Testing. *NSWCCD-65-TR-2005/24*.

[49] Crane, R.M., Ratcliffe, C.P., Gould, R. & Forsyth, D.S. (2006). Comparison Of The Structural Irregularity And Damage Evaluation Routine (SIDER) Inspection Method With Ultrasonic And Thermographic Inspections To Locate Impact Damage On An A-320 Vertical Stabilizer. *Proceedings of the 33rd Annual Review of Progress in Quantitative Nondestructive Evaluation*, July 30 - Aug 4, 2006, Portland, OR.

[50] Irwin. G. (1957). Analysis of Stresses and Strains Near the End of a Crack Traversing a Plate. *J. Appl. Mech.*, *24*, 361-364.